

---

## Understanding the mechanical properties of novel UHTCMCs through random forest and regression tree analysis

Antonio Vinci <sup>a</sup>  , Luca Zoli <sup>a</sup> , Diletta Sciti <sup>a</sup> , Cesare Melandri <sup>a</sup> , Stefano Guicciardi <sup>b</sup> 

<https://doi.org/10.1016/j.matdes.2018.02.061>

### Highlights

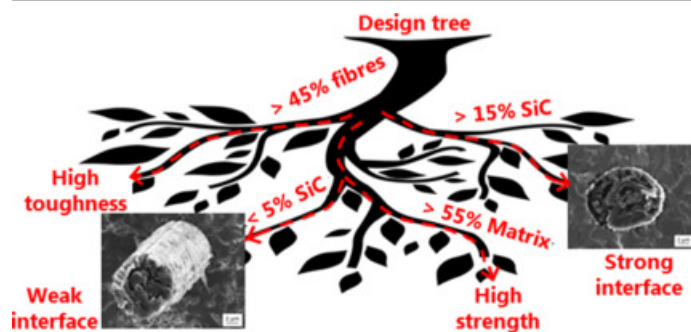
- The mechanical properties of ZrB<sub>2</sub>/SiC-Cf composites were investigated.
- The most important parameter is the ratio between SiC and fibre content.
- High strength and toughness are achieved for high SiC/fibre ratio.
- Higher SiC contents promote a stronger fibre/matrix interface but limit pull-out.

### Abstract

The microstructure and the mechanical properties of ZrB<sub>2</sub>-SiC-Cf [ceramic composites](#) were investigated. The SiC phase, whose amount was varied from 5 to 20 vol%, was introduced in order to improve the densification, [oxidation resistance](#) and mechanical properties of the composite. The microstructure was analysed by SEM-EDS and image

analysis. Increasing the amount of SiC from 5 to 20 vol% resulted in an improvement of the materials density, from 90% to 94%. The non-brittle 4-pt **flexural strength** ranged from 164 to 247 MPa, with no clear dependence on the amount of SiC added. The same holds true for the fracture toughness, ranging from 4.8 to 8.4 MPa·m<sup>0.5</sup>. In order to track the most important microstructural parameters affecting the properties, experimental data were analysed with the Random Forest and Regression Tree statistical models. The statistical analysis demonstrated that among the possible explanatory variables such as porosity, amount of SiC, fibre content, matrix content, SiC/fibre amount ratio, the one having a major influence on both the flexural strength and fracture toughness is the ratio between SiC and **carbon fibre** content.

## Graphical abstract



[Download high-res image \(120KB\)](#)

[Download full-size image](#)

## Keywords

Ceramic-Matrix Composites (CMCs); Mechanical properties; Statistical methods; Ultra-High-Temperature-Ceramics (UHTCs); Fibre-matrix interface; Zirconium diboride

## 1. Introduction

Ultra-High-Temperature-Ceramics (UHTCs), such as **transition metal** diborides, are a novel class of materials characterized by melting points exceeding 3000 °C, high thermal and electrical conductivity and good ablation resistance [1]. Among UHTCs, ZrB<sub>2</sub>-based ceramics have been investigated as potential candidates for the fabrication of reusable Thermal Protection Systems (TPS) for aerospace applications owing to their high **thermal conductivity** and relatively low density [1,2]. However, their low fracture toughness and poor **thermal shock resistance** pose major obstacles to their implementation [3]. Moreover, the **oxidation resistance** of ZrB<sub>2</sub> is low at temperatures above 1200 °C due to the formation of volatile **oxides** (B<sub>2</sub>O<sub>3</sub>) that leave behind a non-protective porous scale of ZrO<sub>2</sub> [4]. The addition of **silicon carbide** up to 30 vol% has been found to aid the **sintering** of ZrB<sub>2</sub> and to increase its oxidation resistance due to the formation of a viscous **borosilicate glass** with low vapour pressure [[5], [6], [7], [8]]. Common routes to the sintering of UHTCs are **hot pressing** (HP), pressure-less sintering (PS), **spark plasma sintering** (SPS) and reactive hot pressing (RHP) [9,10]. Even though pressure-less sintering is an

attractive route for the fabrication of more complex shapes, hot pressing remains the preferred route because of the high relative density of the final composite. The materials currently used in aerospace environments, based on C/C, SiC/SiC or C/SiC **ceramic composites**, display excellent **thermomechanical properties** but **carbon fibres** start oxidizing at temperatures as low as 500 °C, while SiC becomes chemically active above 1650 °C, resulting in high ablation rates and the **sublimation** of the ceramic matrix. By combining the good ablation resistance of a UHTC matrix and the high **damage tolerance** provided by carbon fibres, the above mentioned limits could be overcome.

Previous works done by Corral et al. [11] on UHTC coatings demonstrated the increase of ablation and oxidation resistance of C/C composites, while Tang et al. [11,12] achieved increased oxidation resistance by embedding 4–18 vol% of ZrB<sub>2</sub> particles in a C/SiC composite due to the synergy between B<sub>2</sub>O<sub>3</sub> and SiO<sub>2</sub> that form a protective borosilicate glass.

In the past few years, a new class of materials labelled UHTCMCs (Ultra High Temperature Ceramic Matrix Composites) has been developed that consists of a UHTC rich matrix reinforced with carbon fibres. The main limitation lies in the difficult infiltration of long fibres with the ceramic powders suspensions and the densification of the final composite. Sciti et al. [[13], [14], [15]] successfully sintered UHTCMCs without the aid of expensive techniques such as CVI or PIP, by employing **slurry** infiltration coupled with vacuum bagging and hot pressing. Preliminary studies on the oxidation behaviour of these composites have shown their promising oxidation resistance up to 1500 °C [16], but no mechanical characterization has been carried out.

In this work, carbon fibre reinforced ZrB<sub>2</sub>/SiC composites were fabricated by slurry infiltration and hot pressing. SiC was added in amounts ranging from 5 to 20 vol%, while carbon fibre content was varied between 35 and 50 vol%. Due to process limitations, such as powder suspension rheology, it was difficult to adjust the fibre content for some compositions. Pitch fibres were chosen on the basis of previous studies by Silvestroni et al. [17] that showed the different reactivity of fibres with the surrounding ceramic matrix. The aim of this work is to investigate the mechanical behaviour of ZrB<sub>2</sub>/SiC composites and identify the key parameters affecting mechanical properties. Two machine learning techniques, Random Forest and Regression Tree, were employed in order to rank the key explanatory variables and quantify their effects on the mechanical properties [18]. These techniques are widely applied in several fields like ecology [[19], [20], [21], [22]], medicine [[23], [24], [25], [26]] or sociology [[27], [28], [29], [30]]. Few examples can be also found in material science [31,32].

## 2. Experimental

### 2.1. Materials

Commercially available powders were used for the fabrication of **ceramic composite materials**: ZrB<sub>2</sub> (H.C. Starck, grade B, Germany, specific surface area 1.0 m<sup>2</sup>/g, particle size range 0.5–6 µm, impurities (wt%): 0.25C, 2 O, 0.25 N, 0.1 Fe, 0.2 Hf), α-SiC (H.C. Starck, Grade UF-25, Germany, specific surface area 23–26 m<sup>2</sup>/g, D50 0.45 µm Italian retailer: Metalchimica). Unidirectional high modulus **carbon fibres** (Granoch Yarn XN80-6K fibres; **tensile modulus** of 780 GPa and **tensile strength** 3.4 GPa, 10 µm diameter. Supplier: Angeloni) were used as carbon preforms.

### 2.2. Process

Powder mixtures containing ZrB<sub>2</sub> and SiC ranging from 5 to 20 vol% were prepared by wet ball milling of the commercial powders and then dried with a rotary evaporator. The composites were prepared through **slurry** infiltration of unidirectional carbon fibre preforms and hand lay-up in a 0–90° configuration. **Hot pressing** cycles were carried out at 1900 °C, using a pressure of 40 MPa and a holding time of 10 min, on the basis of previous studies [13]. For each composition, three variants, a, b and c, were fabricated by adjusting the powder suspension rheology according to three fixed values labelled as a,b,c (not explicitly indicated in this work). In order to obtain different contents of carbon fibres. Due to process limitations, it was not possible to obtain fibre contents higher than 40% for some compositions as shown in **Table 1**.

Table 1. **Flexural strength** (mean ± 1 standard deviation) and physical characteristics of samples ZS5, ZS10, ZS15, ZS20.

	$\sigma$ (MPa)	Density (g/cm <sup>3</sup> )	Porosity (vol%)	Fibre (vol%)	Matrix (vol%)	SiC/fibre Ratio	SiC vol% in matrix
ZS5 a	198 ± 12	3.649	12.9	40.7	46.4	0.123	5
ZS5 b	207 ± 24	4.194	7.2	35.2	57.6	0.142	5
ZS5 c	247 ± 14	4.055	9.5	35.4	55.2	0.141	5
ZS10 a	218 ± 30	3.616	9.5	45.2	45.3	0.221	10
ZS10 b	171 ± 1	4.205	4.1	37.7	58.2	0.265	10
ZS10 c	196 ± 28	3.864	9.8	37.8	52.3	0.264	10
ZS15 a	190 ± 33	3.315	10.2	50.8	39.0	0.295	15
ZS15 b	167 ± 4	3.617	6.4	48.2	45.3	0.311	15
ZS15 c	186 ± 49	3.952	7.5	36.9	55.6	0.406	15
ZS20 a	221 ± 19	3.391	8.7	49.3	42.0	0.405	20
ZS20 b	247 ± 12	3.762	6.0	42.7	51.3	0.468	20
ZS20 c	164 ± 2	4.003	5.4	36.6	58.1	0.547	20

### 2.3. Microstructure analysis

The microstructure was analysed on polished and fracture surfaces by [field emission scanning electron microscopy](#) (FE-SEM, Carl Zeiss Sigma NTS GmbH Oberkochen, Germany) and [energy dispersive X-ray spectroscopy](#) (EDS, INCA Energy 300, Oxford instruments, UK). For each composition, three pellets (variants) were prepared by varying the fibre content from 35 to 50% and maintaining the hot pressing parameters unchanged. Samples were prepared for microscopy by cutting cross sections, mounting them in epoxy [resin](#), and then polishing down to a 0.25  $\mu\text{m}$  finish with diamond [abrasives](#), using semi-automatic polishing machine (Tegramin-25, Struers, Italy). The polished samples were then washed with ethanol in an ultrasonic bath, dried under IR light and cleaned with a plasma cleaner (Colibri Plasma RF 50 kHz, Gambetti, Italy) at 40 W for 5 min. The starting compositions (e.g. the fibre and matrix volumetric amounts) were estimated in different steps. Before [sintering](#), the green pellet was weighted and the fibre volumetric amount was determined taking into account the fibre areal weight ( $\text{g}/\text{m}^2$ ) given by the supplier, number of layers and sample area. The matrix amount was then determined as the difference between the total pellet weight and the fibre weight. Hence, a theoretical density of the materials based on the initial composition was calculated using the rule of mixture. After sintering, the geometric density and porosity were estimated.

### 2.4. Mechanical properties

Four points [bending strength](#) tests were carried out on test bars  $25 \times 2.5 \times 2 \text{ mm}^3$  (length by width by thickness, respectively) using a semi-articulated [silicon carbide](#) four-point fixture with a lower span of 20 mm and an upper span of 10 mm using a screw-driven testing machine (Zwick/Roell, model Z050), following the guidelines of standard ISO 14704:2016(en). For each material at least three bars were tested and the [flexural strength](#) was calculated as the bars were made of a homogeneous material. Although for these kind of composites the standards suggest a Span/thickness (S/t) ratio higher than 20, for this preliminary study and comparison purposes we opted for the production of small bars. In addition, tests done with larger bars and  $S/t = 20$  demonstrated that the maximum flexural stress was very similar in value and the fracture mode was still mixed.

The fracture toughness ( $K_{Ic}$ ) was evaluated by four-point chevron notch bending tests (CNB). The test bars were 25 mm × 2 mm × 2.5 mm<sup>3</sup> (length by width by thickness, respectively) and were notched with a 0.1 mm-thick diamond saw; the chevron-notch tip depth and average side length were about 0.12 and 0.80 of the bar thickness, respectively. The specimens were fractured using a fully-articulated **steel** four-point fixture with a lower span of 20 mm and an upper span of 10 mm using a screw-driven testing machine (Zwick/Roell, model Z050). Three specimens were loaded with a crosshead speed of 0.05 mm/min. The “slice model” equation of Munz et al. [33] was used to calculate  $K_{Ic}$ .

## 2.5. Statistical analysis

Since there is no parametric model which relates the mechanical response variable, strength or fracture toughness, to the microstructural features, in the following, two non-parametric learning machine techniques, Regression Tree and Random Forest, will be considered in order to establish quantitative relationships between the response variables and the predictor variables. Regression tree analysis is a simple non-parametric machine learning techniques that is based on the recursive partitioning of the each explanatory variables and then calculating the residual sum of squares (RSS) of the two corresponding groups of the response variable values [16]. The most important explanatory variable  $x_i$  is that whose cutpoint  $x_c$  minimizes the RSS (Eq. (1)):

$$RSS = \sum_j^{n_1} (y_{j1} - \bar{y}_1)^2 + \sum_j^{n_2} (y_{j2} - \bar{y}_2)^2 \quad (1)$$

where  $y_{j1}$  and  $y_{j2}$  are the response variable values corresponding to the explanatory variable values  $<x_c$  and  $\geq x_c$ , respectively, and  $\bar{y}_1$  and  $\bar{y}_2$  are the group means. The process is then repeated. The research of further split stops according to some criterion such as the minimum number of response values to split or the depth of the tree. Moreover, to avoid overfitting, pruning is applied in order to obtain the optimal tree. The optimal tree is the smallest tree that has near minimum cross-validated relative error. The regression tree method has several advantages with respect to other more common statistical techniques like regression [34]: 1) trees do not require the user to specify the model in advance, 2) trees use automatic feature selection, which allows the approach to be used with a very large number of features, 3) trees are adept at capturing nonlinear or non-additive behaviour as interactions are automatically included, 4) trees are very easy to explain and can be displayed graphically.

The algorithm on which the regression tree is based is greedy in the sense that is optimal for the first split but does not look ahead to see if different ways of splitting are better at the end. Random Forest is an evolution of the tree-based model [35]. A Random Forest is generated by growing many full (no pruning) trees, usually  $\geq 500$ , using a random subset of the explanatory variables for each tree and for each split. This method is trained on a subset, usually 2/3, of the response variable values with the remaining 1/3 used for testing. A single regression tree will obtain a single prediction result with a single input vector. However, a Random Forest will obtain multiple results from a single input as it grows many regression trees. Therefore, a Random Forest will use an average output for the prediction result of the regression with increased reliability [36]. A Random Forest model cannot be displayed graphically, however a plot of the importance of the explanatory variables on the mean square error (MSE) can be obtained.

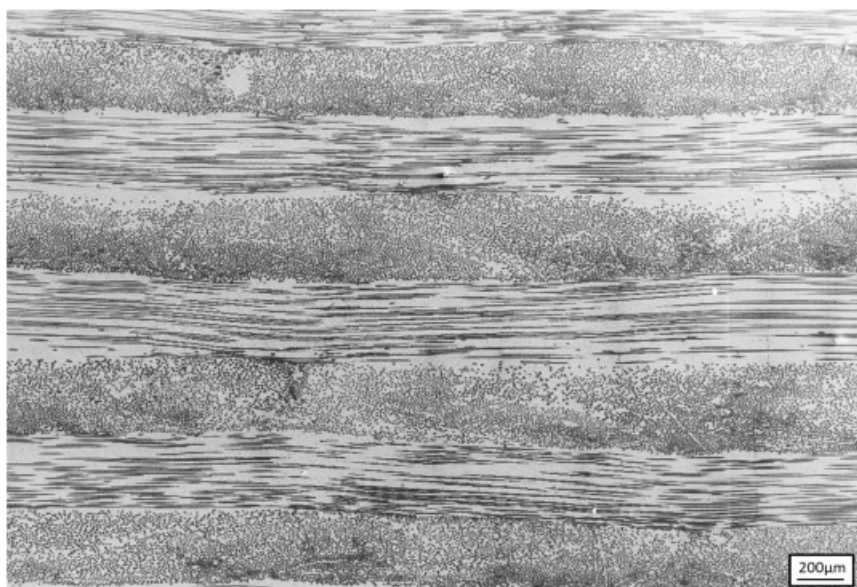
In this section we have presented the Regression Tree first and Random Forest after. However, for a more logical procedure, in the Results section we will present first the Random Forest analysis, to show which are the most important explanatory variables, and then the Regression Tree analysis to analytically display the impact of the explanatory variables on the response variable.

## 3. Results and discussion

### 3.1. Microstructure of the sintered material

For each composition, three composites (variants) were prepared by varying the **slurry** viscosity between three fixed values, in order to obtain different **carbon fibre** contents: a (highest fibre amount), b (intermediate fibre amount), c (lowest fibre amount). In some cases it was not possible to go beyond a specific fibre content due to the fact that the

sole change of SiC content strongly modifies the slurry viscosity, therefore some variants (namely, b and c) may exhibit similar physical properties, see [Table 1](#). Typical defects of these composites are non-infiltrated areas and cracks in the matrix-rich regions. Cracks originate from the constrained shrinkage of the ceramic matrix during [sintering](#) and the mismatch between the thermal expansion coefficients of matrix and fibres ( $6.5 \cdot 10^{-6} \text{ K}^{-1}$ ,  $2 \cdot 10^{-6} \text{ K}^{-1}$ , respectively [4]). As an example, the low magnification micrograph of the sample ZS5 c is shown in [Fig. 1](#).



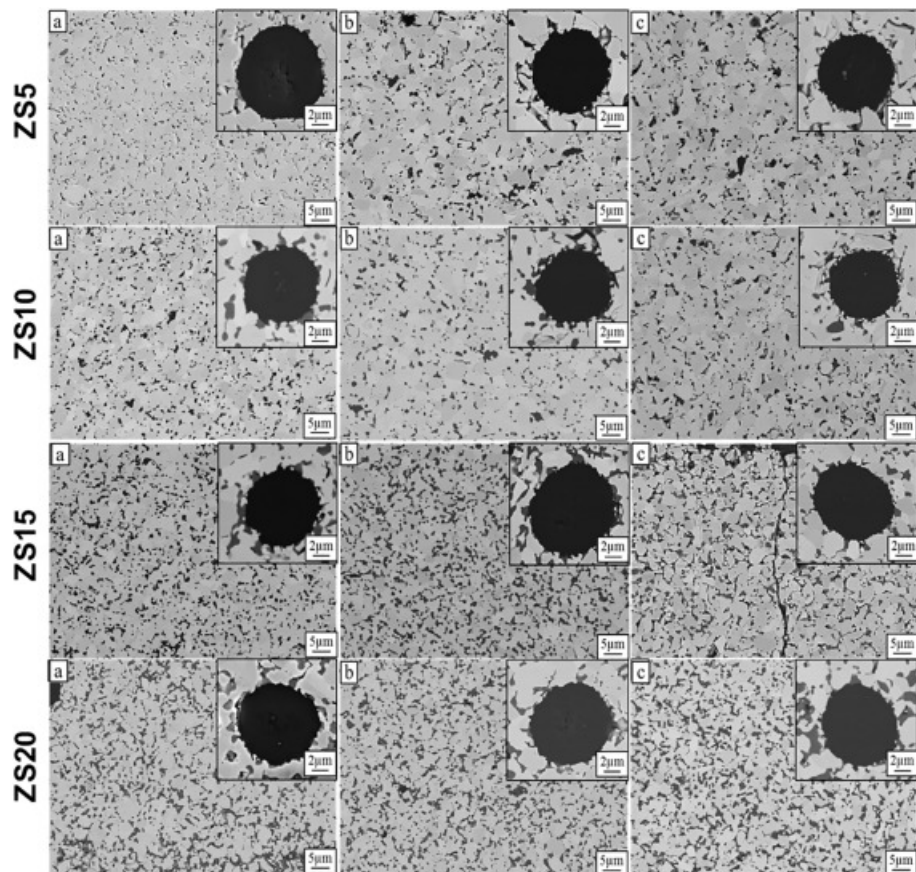
[Download high-res image \(550KB\)](#)   [Download full-size image](#)

Fig. 1. Low magnification micrograph of the 0/90° fibre orientation of sample ZS5 c. Carbon fibres are represented in black and the ceramic matrix in light grey.

The light grey phase comprises the ceramic matrix consisting of  $\text{ZrB}_2$ -SiC, while the black phases are carbon fibres stacked with a 0/90° orientation. It was possible to achieve a homogeneous infiltration of fibres for the composites with a fibre content higher than 40 vol%, whereas for high solid loading suspensions homogeneous infiltration of single fibre bundles was hardly achieved. In addition, UHTC composites are difficult to sinter, due to both the low sinterability of the matrix and presence of large amounts of C fibres constraining the matrix shrinkage. A porosity <5 vol% was achieved only for the samples with a SiC content  $\geq 10$  vol%, owing to SiC capability of aiding the sintering of  $\text{ZrB}_2$  via [liquid phase sintering](#) [37].

[Fig. 2](#) shows the microstructure of the carbon fibre section of each sample. The samples were labelled as ZS# a,b,c, where # is the volumetric SiC content. The light grey regions represent  $\text{ZrB}_2$ , while SiC particles comprise the majority of dark grey phases. For low amounts of SiC, it is possible to observe the homogenous dispersion of fine particles in the ceramic matrix and around the carbon fibres, while increasing the SiC content above 15 vol% results in the agglomeration of the finer SiC particles. Carbon fibres do not show significant signs of reaction with the ceramic matrix and maintain their original round shape, in agreement with previous studies on pitch carbon fibres [17]. Samples with high ceramic matrix content, e.g. ZS15 c ([Fig. 1](#)), are characterized by the presence of cracks, while the other samples do not show relevant defects. The average  $\text{ZrB}_2$  particle size is in the range 2.5–3  $\mu\text{m}$  in all samples, as ascertained by image analysis, with a slight decrease in size for higher SiC contents. This could be due to

the high amount of fibres in all specimens that is the main responsible for the hindered grain growth of  $ZrB_2$ . As for the matrix fibre interface, since no coating was adopted for the fibres, the interface was generally quite strong due to a good adhesion between the boride and the fibre layers. Of the four different compositions, the weaker interface was that of ZS5 due to slightly lower degree of densification of the matrix, in agreement with previous studies [13].



[Download high-res image \(691KB\)](#)   [Download full-size image](#)

Fig. 2. High magnification micrographs of the ceramic matrix of samples ZS5-20 a, b and c. In the insets, a magnification of a corresponding carbon fibre section with the surrounding matrix phase.

### 3.2. Flexural strength

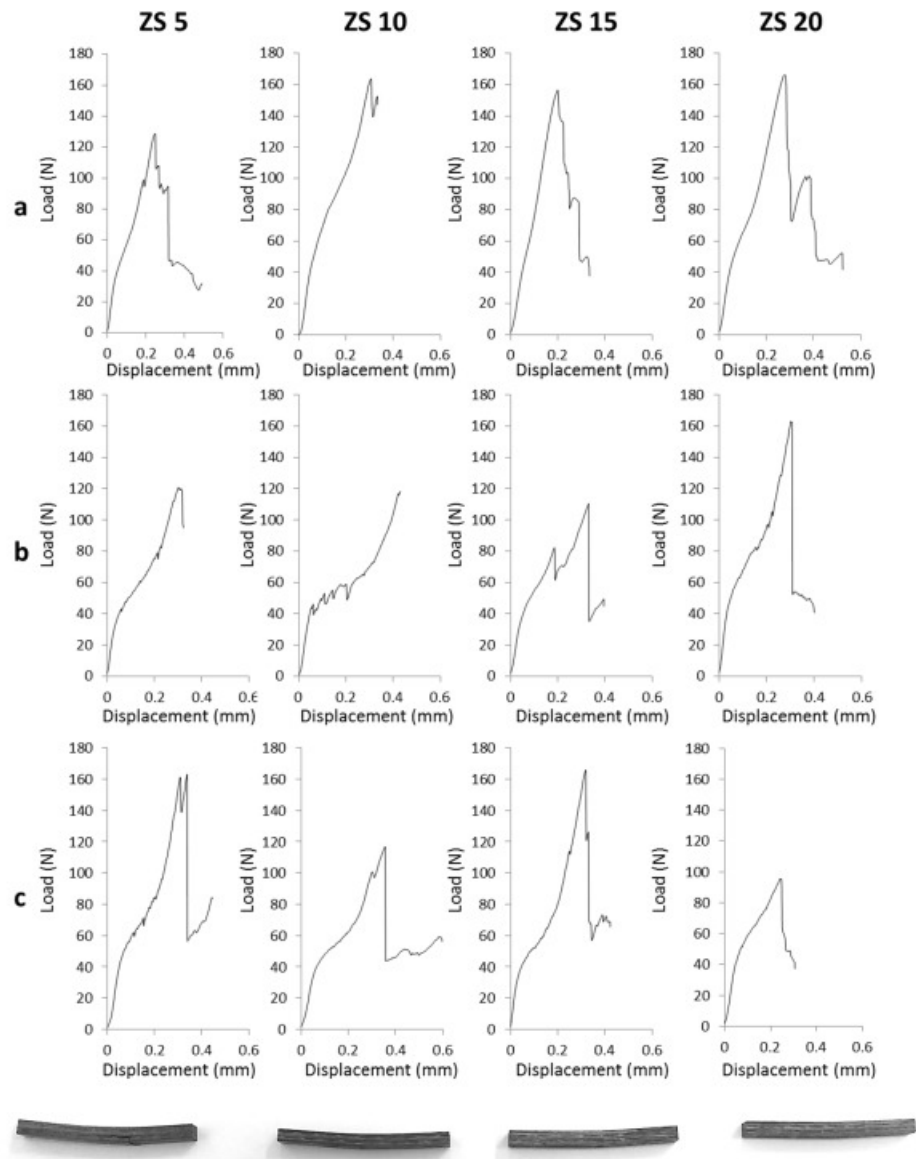
For each bar, the geometric density, porosity, fibre vol%, ceramic matrix vol%, fibre/SiC ratio and layer thickness were measured. Results are reported in [Table 2](#).

Table 2. Fracture toughness and physical characteristics of samples ZS5, ZS10, ZS15 and ZS20. ZS10 c was not reported due to insufficient data.

	$K_{Ic}$ (MPa·m <sup>0.5</sup> )	Density (g/cm <sup>3</sup> )	Porosity (vol%)	Fibre (vol%)	Matrix (vol%)	SiC/fibre ratio	SiC vol% in matrix
<b>ZS5 a</b>	4.75 ± 0.31	3.614	13.5	40.7	45.8	0.123	5
<b>ZS5 b</b>	7.02 ± 0.49	4.038	9.9	35.2	54.9	0.142	5
<b>ZS5 c</b>	5.20 ± 0.58	4.013	10.2	35.4	54.5	0.141	5
<b>ZS10 a</b>	6.13 ± 0.30	3.619	9.4	45.2	45.4	0.221	10
<b>ZS10 b</b>	6.39 ± 1.29	4.084	6.1	37.7	56.2	0.265	10
<b>ZS15 a</b>	8.35 ± 0.98	3.212	12.0	50.8	37.2	0.295	15
<b>ZS15 b</b>	5.52 ± 0.94	3.521	8.1	48.2	43.6	0.311	15
<b>ZS15 c</b>	6.33 ± 0.44	3.886	8.7	36.9	54.4	0.406	15
<b>ZS20 a</b>	6.93 ± 0.43	3.238	11.4	49.3	39.2	0.405	20
<b>ZS20 b</b>	6.68 ± 0.94	3.749	6.2	42.7	51.1	0.468	20
<b>ZS20 c</b>	5.01 ± 0.90	3.849	8.1	36.6	55.3	0.547	20

All samples display quasi-brittle [fracture behaviour](#) and the two halves of the specimen remain connected after the tests as shown in [Fig. 3](#). Because of the low span/thickness ratio, the failure modes were caused by flexural yield, inter-laminar shearing or a combination of the two. Inter-laminar shear failure is characterized by the opening of a void between the planes, while flexural yield failure is characterized by fibre rupture, which may result from plane bending. During the first part of the load-displacement curve, stresses are mainly concentrated on the ceramic matrix. As the load increases, cracks start to open in the ceramic matrix and the load is transferred to the fibres. [Delamination](#) may occur, as evidenced in some curves by the drop in applied load and the re-loading of the second layer.





[Download high-res image \(283KB\)](#)   [Download full-size image](#)

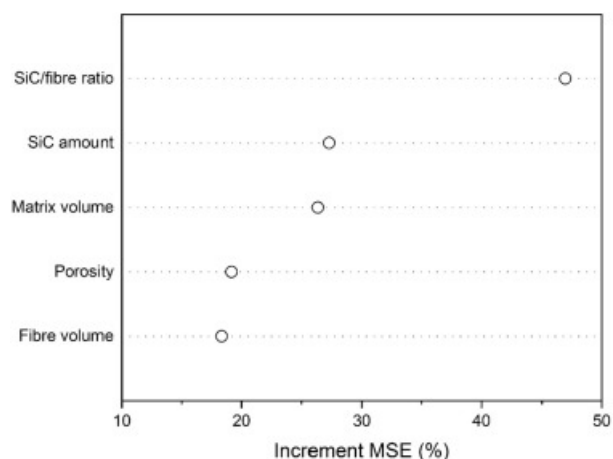
Fig. 3. Load-displacement curves of 4-point bending tests for samples ZS5, ZS10, ZS15, ZS20 a,b,c. For each sample, only one curve is reported since all bars within the same sample display the same behaviour. At the bottom of the graphs, a lateral view of the specimens after test is shown.

The strength values obtained in this work ranging between 160 and 250 MPa are lower than those reported in literature for typical bulk ZrB<sub>2</sub>/SiC composites, which are in the range of 400–700 MPa [4,[38], [39], [40], [41], [42]]. This could be due to the internal defects brought by the introduction of carbon fibres in the ceramic matrix and the cracks generated due to CTE mismatch between the fibres and the matrix during **hot pressing**. Another reason could lie in the low interfacial strength between each layer which causes the sample to fail prematurely to inter-laminar shear stresses. A way to overcome this issue is the use of three-dimensional **fibre reinforcements**, which is however out of the scope of the present work.

According to previous works by Fahrenholtz et al. on the influence of SiC content on ZrB<sub>2</sub>-SiC bulk ceramics [38], **flexural strength** is expected to increase with increasing SiC content from 10% to 30 vol% due to refinement of ZrB<sub>2</sub> mean grain size and the decrease of porosity. In our materials, with embedded carbon fibres, there is not a clear correlation between the apparent flexural strength and SiC content. High values of strength were obtained for both compositions with 5 and 20 vol% SiC; moreover, the grain size for all the samples is in the range of 2.1–2.8 μm, with a very slight decrease with the increase of SiC content; in this case, the fibres themselves act as the main obstacle to grain growth and the problem related to the potential presence of SiO<sub>2</sub> is overcome thanks to the abundance of carbon from the carbon of fibres that can react to give SiC according to the reaction [43]:



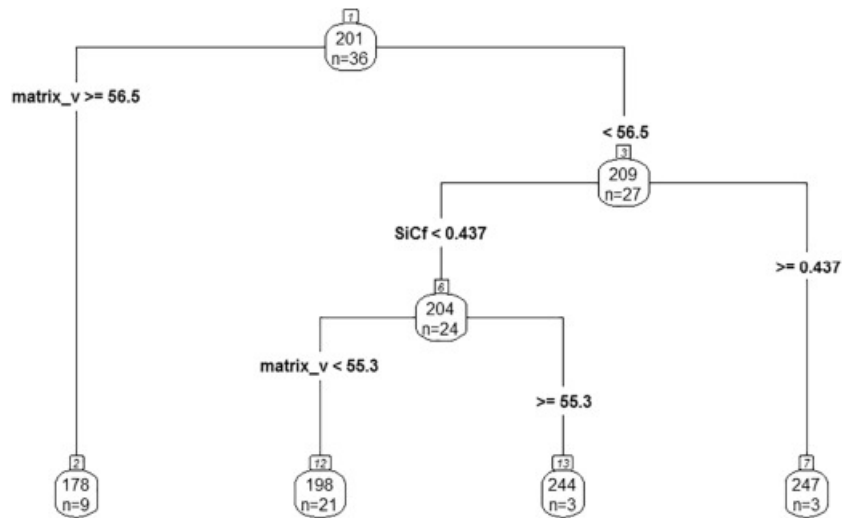
Due to the large number of factors influencing the apparent flexural strength of these materials, Random forest and Regression Tree Analysis were employed in order to identify the key explanatory variables. The following variables were chosen as explanatory variables: 1) the starting nominal amount of SiC particles with respect to the matrix and ranges from 5 to 20% (SiC amount), 2) the fibre volume (Fibre volume), 3) the ratio between the volume of SiC in the matrix and carbon fibre content (SiC/fibre ratio), 4) the overall volumetric amount of ceramic matrix (Matrix volume) and 5) the geometrical porosity across the sample calculated as the ratio between experimental and theoretical geometrical density (Porosity). **Fig. 4** shows the result of the explanatory variable importance according to Random Forest. As the plot indicates, the SiC/fibre ratio is the most important explanatory variable as its removal increments the mean square error (MSE) of about 46%. SiC amount and matrix volume follow with a lower influence. Finally, porosity and fibre volume seem to affect less the strength.



[Download high-res image \(52KB\)](#) [Download full-size image](#)

Fig. 4. Plot of the importance of the explanatory variables on the flexural strength according to the Random Forest analysis. The importance is based on the increment of the mean square error (MSE) due to the removal of the corresponding explanatory variable.

After this, a Regression Tree analysis was carried out in order to quantify the effect of each explanatory variable has on the apparent flexural strength and eventually identify potential correlations between the explanatory variables selected, see Fig. 5. In this plot, in each node, the mean value of the response variable and the number of values are indicated. For example, at node 1 the mean of all the strength value is 311 MPa and the initial number of all the data is 36.



[Download high-res image \(56KB\)](#) [Download full-size image](#)

Fig. 5. Regression tree analysis for the flexural strength. In each node, the mean strength and the number of values is reported. The value on top (201 MPa) is the average flexural strength of all the specimens (36). The condition for the split of the explanatory variable is indicated on the left branch below each node. The explanatory variables are ranked in order of importance from top to bottom with the following abbreviations: matrix\_v = matrix volume, SiCf = SiC/fibre ratio. A final node (leaf) is where the split constrains prevent a further split. See text for a more detailed explanation.

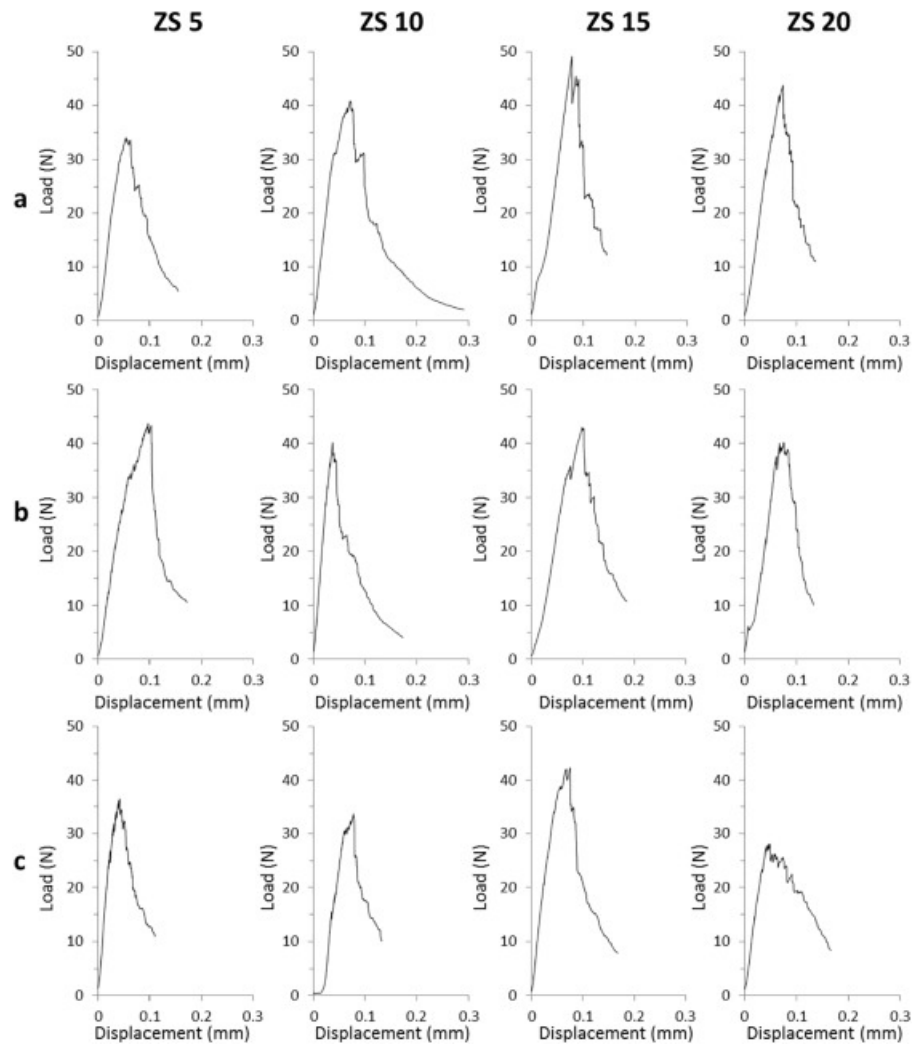
The first split is made according to the most important explanatory variable as calculated by Regression Tree and is indicated on the left branch, which is the matrix volume in this case. If the matrix volume is equal or higher than 56.5 vol%, then the mean strength is 178 MPa, as indicated by the leftmost final node (leaf), calculated on nine values. This is also the lowest mean strength value of all the split groups. When the matrix volume is lower than 56.5 vol%, right branch from node 1, the mean values, calculated on 27 values, is 209 MPa, see node 3. In this case, the data can be split according to the explanatory variable SiC/fibre ratio. If the SiC/fibre ratio is equal or higher than 0.437, right branch, the mean strength is 247 MPa, node 7 (leaf). This is the highest mean strength value of all the split groups. If the SiC/fibre ratio is lower than 0.437, left branch, then the mean strength is 204 MPa. This group can be further split according to the matrix volume: if <55.3 vol%, the mean strength is 198 MPa, node 12 (leaf); if equal or higher than 55.3 vol%, the mean strength is 244 MPa, node 13 (leaf).

We can see that in the Regression Tree analysis, the most important variable is the matrix volume followed by the SiC/fibre ratio. This is a rank inversion with respect to the Random Forest analysis, which should be however considered more reliable. Combining the main results of the Random Forest analysis and those of the Regression Tree, a low matrix volume and a high SiC/fibre ratio are necessary in order to obtain a high-strength composite. The first indication is clearly due to the lower strength of the matrix with respect to that of the fibres. The second indication comes from the observation that there must be a right amount of SiC around the fibres to promote a proper fibre/matrix interface through the reaction of the SiO<sub>2</sub> present on the SiC powders with the carbon fibre [43]. The fracture properties of the fibre composites are known to be strongly dependent on the fibre/matrix interface [44].

### 3.3. Fracture toughness

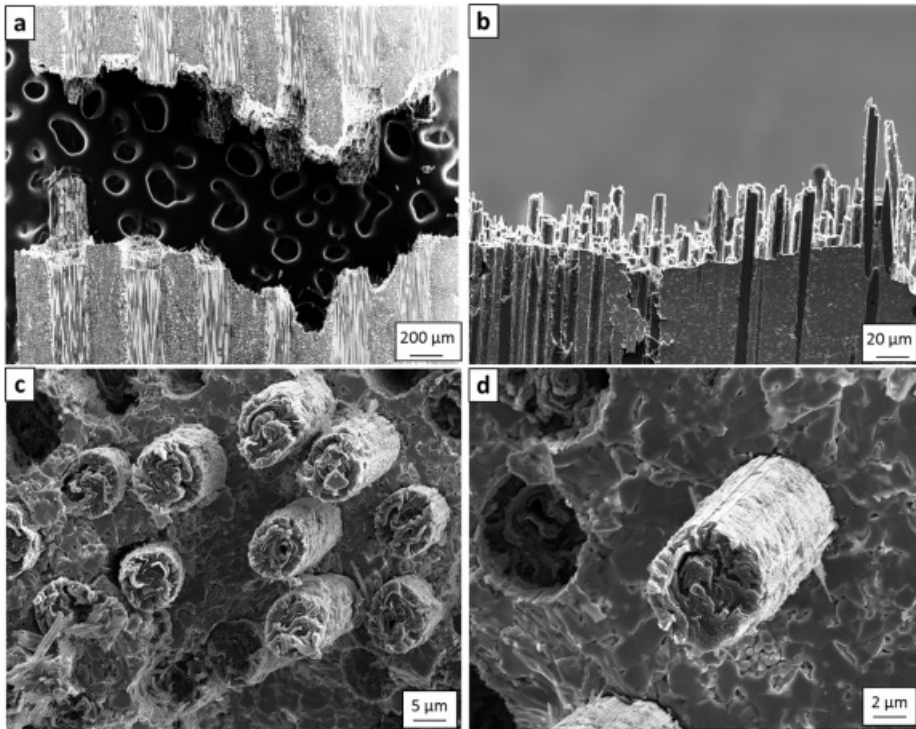
The average values of fracture toughness are reported in Table 2. The fracture toughness of the group ZS10 c was not evaluated.

Typical fracture toughness values for bulk ZrB<sub>2</sub>/SiC composites are in the range of 2–5 MPa·m<sup>0.5</sup>, determined with single edge or chevron notch beam tests [45,46], which increase up to 6.16 MPa·m<sup>0.5</sup> with the introduction of 30% of carbon fibres [47]. Values of indentation toughness up to 7.52 MPa·m<sup>0.5</sup> have been obtained by Guo with the introduction of carbon spheres [48]; however in the present work, due to significant amount of porosity and matrix discontinuity, the indentation-induced cracks are hardly observable and misleading. For the materials of the present work, the fracture toughness ranged from 4.75 to 8.35 MPa·m<sup>0.5</sup>. The load-displacement curves display quasi-brittle fracture behaviour, Fig. 6. All samples exhibit very similar behaviours. An example of fracture surface is shown in Fig. 7, which reveals both fibre bundle pull-out and individual fibre pull-out. The extent of fibre pull-out should be strictly related to the cohesion between matrix and fibre that develops during the densification process. High temperatures and holding times during hot pressing will lead to significant reaction between carbon fibres and the ceramic matrix, which results in too strong interfaces and brittle behaviour [49]. Previous studies from Hong et al. [50] showed a degradation of the mechanical properties with the increase of short carbon fibre content from 20 to 50%, but in our case there is not a clear correlation between fracture toughness and carbon fibre content, which is likely due to the different effect of continuous fibres.



[Download high-res image \(228KB\)](#) [Download full-size image](#)

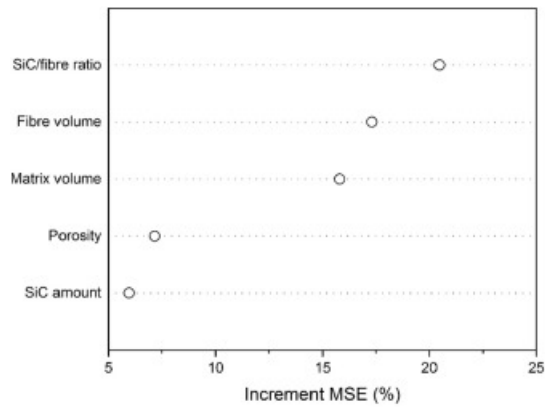
Fig. 6. Load-displacement curves of 4-point Chevron notch bending tests of samples ZS5, ZS10, ZS15, ZS20. For each sample, only one curve is reported since all bars within the same sample display the same behaviour.



[Download high-res image \(527KB\)](#)   [Download full-size image](#)

Fig. 7. Fracture surfaces of sample ZS5c: a) Fracture profile and fibre bundle pull-out, b) Fibre pull-out profile view, c) Fibre pull-out section view, d) Individual fibre pull-out.

The same explanatory variables used for the strength were considered for  $K_{IC}$ . The Random Forest results regarding the importance of these explanatory variables are shown in Fig. 8.

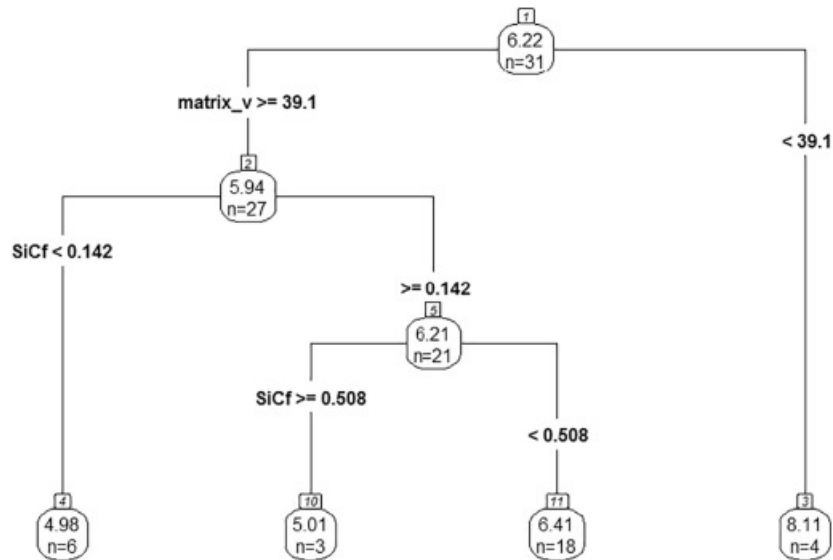


[Download high-res image \(46KB\)](#) [Download full-size image](#)

Fig. 8. Plot of the importance of the explanatory variables on the fracture toughness according to the Random Forest analysis. The importance is based on the increment of the mean square error (MSE) due to the removal of the corresponding explanatory variable.

Even for fracture toughness, the ratio between SiC and carbon fibre emerges as the most important explanatory variable by the RF analysis. However, in this case the SiC/fibre ratio is followed by the fibre volume and matrix volume. Porosity and SiC amount are the least influencing explanatory variables.

The Regression Tree analysis is shown in Fig. 9. Differently from the RF analysis, the most important explanatory variable was the matrix volume. The highest mean value of  $K_{Ic}$  is obtained for a matrix volume <39.1 vol%,  $8.11 \text{ MPa}\cdot\text{m}^{0.5}$ . For matrix volume higher than 39.1 vol%, the toughness drops to a mean value of  $5.94 \text{ MPa}\cdot\text{m}^{0.5}$ . This last group can be however further split according to the SiC/fibre ratio values, which means an interaction between the two explanatory variables matrix volume and SiC/fibre ratio. For a SiC/fibre ratio lower than 0.142, the mean fracture toughness was the lowest of all the split groups,  $4.98 \text{ MPa}\cdot\text{m}^{0.5}$ . When the SiC/fibre ratio was equal or higher than 0.142, the mean fracture toughness was  $6.21 \text{ MPa}\cdot\text{m}^{0.5}$ . In turn, the latter group can be again split according to the same explanatory variable, i.e. the SiC/fibre ratio. In this case, there is an apparent optimal SiC/fibre ratio range: high values of fracture toughness are obtained when this ratio is between 0.142 and 0.508, mean fracture toughness of  $6.41 \text{ MPa}\cdot\text{m}^{0.5}$ . For SiC/fibre ratio higher than 0.508 the mean fracture toughness is  $5.01 \text{ MPa}\cdot\text{m}^{0.5}$ .



[Download high-res image \(67KB\)](#) [Download full-size image](#)

Fig. 9. Regression tree analysis for the fracture toughness. In each node, the mean fracture toughness and the number of values is reported. The value on top is the average fracture toughness (6.22 MPa·m<sup>0.5</sup>) of all the specimens (31). The condition for the split of the explanatory variable is indicated on the left branch below each node. The explanatory variables are ranked in order of importance from top to bottom with the following abbreviations: matrix\_v = matrix volume, SiCf = SiC/fibre ratio. A final node (leaf) is where the constraints prevent a further split. See text for a more detailed explanation.

The high fracture toughness values associated to a low matrix volume are due to the fact that a low matrix volume corresponds in most cases to a high fibre volume. The SiC/fibre ratio, that was the most important explanatory variable for the apparent flexural strength, is apparently of less importance for fracture toughness even if a strong influence can be observed when the matrix volume was higher than 39.1%.

Since the results of Random Forest are more reliable than those of Regression Tree, we can affirm that to obtain high-toughness composites the SiC/fibre ratio should be primarily controlled followed by the volume of the fibre. As for the strength, the proper interface fibre/matrix is fundamental in determining the fracture behaviour. A too strong interface, as that obtained when the SiC/fibre ratio is higher than 0.508, lowers both strength and fracture toughness as the mechanism of pull-out is ineffective. Following that, a high volume of fibre, i.e. a low matrix volume, positively affects the fracture toughness as well. Considering the flexural strength and the fracture toughness together, it is apparent that the SiC/fibre ratio is the most important explanatory variable for this type of composites.

There is however a minor trade-off between fibre and matrix volume regarding these two mechanical properties. Besides a proper fibre/matrix interface, high-strength composites seem to require a relatively high volume of matrix with respect to the fibre volume, the opposite holds for high-fracture toughness composites.

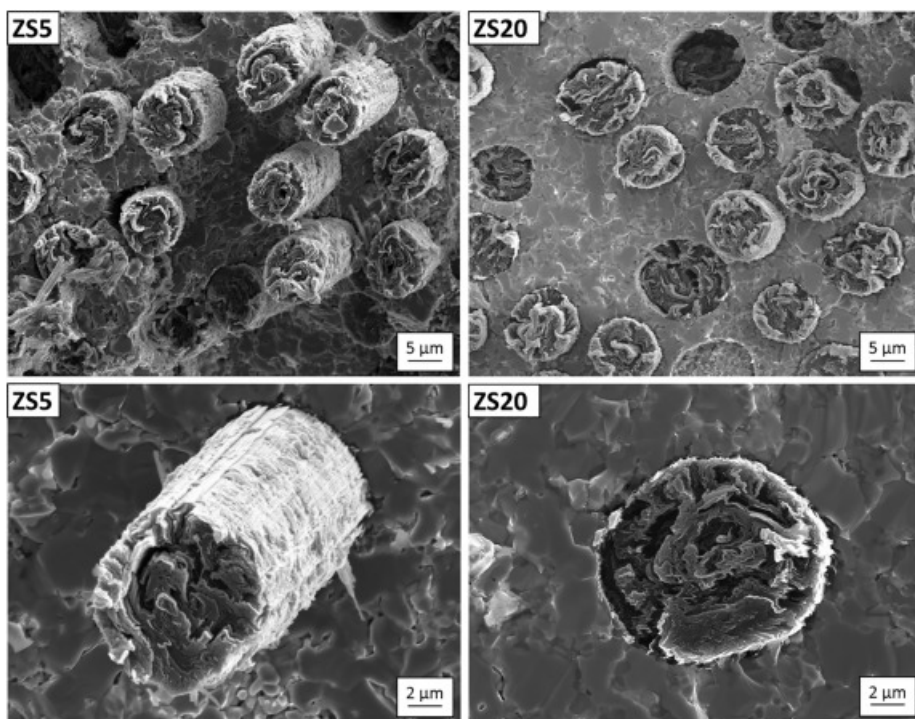
One of the fundamental issues encountered in conventional CMCs based on C/SiC or SiC/SiC is the interface between the fibre and the ceramic matrix. If the interface is too strong, the load is more efficiently transferred from the matrix to the fibres, but this can result in the fibres rupturing together with the matrix, leading to a **brittle fracture**. On the other hand, a weak interface will promote fibre pull-out and trigger other toughening mechanisms such as **crack bridging** or crack deviation. In this regard, carbon and BN



coatings have been studied and applied on SiC or carbon fibres in order to obtain a weak interface and avoid matrix cracks to break through the fibre [[51], [52], [53]]. The main downside to this approach is associated to the weak **oxidation resistance** of the coating at high temperatures that can compromise the mechanical properties of the material, beside the added costs of manufacturing the coated fibres.

Since the SiC/Cf ratio seems to play an important role in the mechanical properties of these composites, the fracture surfaces were studied more in-depth to better understand the interaction of fibres with the interface and the extent of fibre pull-out. Two extreme cases, ZS5c and ZS20c, were taken into consideration to highlight the main difference.

As shown in Fig. 10, the extent of fibre pull-out is visibly more pronounced for the composition with 5 vol% SiC (pull-out extent higher than 10  $\mu\text{m}$ ) which is characterized by lower porosity and a lower degree of reaction at the interface of the fibre with the  $\text{SiO}_2$  impurities. On the other hand, a SiC content of 20 vol% promotes a very dense and strong interface that limits fibre pull-out (pull-out extent  $<1 \mu\text{m}$ ). Bundle pull-out is still present for both compositions. The composites with intermediate amounts of SiC, i.e. 10 vol% and 15 vol%, show very similar fibre/matrix interfaces and pull-out which are difficult to quantify due to the small range of values.



[Download high-res image \(510KB\)](#)   [Download full-size image](#)

Fig. 10. High magnification micrographs of the fracture surfaces of samples ZS5c on the left (weak fibre/matrix interface, higher pull-out) and ZS20c on the right (strong fibre/matrix interface, limited pull-out).

However, an excessively weak interface may lead to poor performance. In the present work it was possible to obtain a fibre pull-out extent up to 20–40  $\mu\text{m}$  with low SiC content, but this in turn results in a weaker ceramic matrix. This may also lower the interfacial strength between each layer and promote delamination during testing [38]. On the other

hand, a higher amount of SiC provides a stronger matrix but limits fibre pull-out. The best compromise can be reached by adjusting process parameters and matrix composition in order to both retain a strong matrix and a good fibre pull-out. In this regard, coated fibres may prove to be the solution and will be object of future works.

#### 4. Conclusions

The microstructure and the mechanical properties of bi-directional **carbon fibre** reinforced UHTCs with varying amount of SiC and carbon fibre were investigated. A statistical analysis based on Random Forest and Regression Tree was carried out to discern the importance and the influence of the explanatory variables (microstructural features) on the response variables (strength or fracture toughness).

In the composites, the fibres were homogenously distributed as well as SiC particles. Grain size was in the range of 2.1–2.8  $\mu\text{m}$  for all samples, with a slight decrease with the increase of SiC content. Initially the microstructure did not show significant signs of reaction with the fibres, but a more in-depth study on the fracture surfaces revealed hindered pull-out for higher amounts of SiC.



All the specimens broke in a quasi-brittle fashion with large evidence of fibre pull-out, either in bundle or singularly. The values of apparent **flexural strength** ranged from 164 to 247 MPa, apparently affected neither by the fibre content nor the SiC content. Both for the apparent flexural strength and the fracture toughness, the most important explanatory variables were the matrix volume and the SiC/fibre ratio. Random Forest ranks the SiC/fibre ratio as first and the matrix volume as second, whereas the Regression Tree ranks the opposite. Combining the results of both the statistical analysis, it can be said that in order to obtain a high-strength high-toughness composite, the composite should have a low volumetric fraction of matrix, and consequently a high amount of fibre, and a high SiC/fibre ratio. The first indication implies a low contribution from the weaker of the two phases making the composite. The second indication points out the importance of having a proper fibre/matrix interface to activate the load-transfer mechanism.

#### Acknowledgements

This work has received funding from the European Union's Horizon 2020 "Research and innovation programme" under grant agreement No. [685594](#) (C<sup>3</sup>HARME).

[Recommended articles](#)   [Citing articles \(1\)](#)






#### References

- [1] M.M. Opeka, I.G. Talmy, E.J. Wuchina, J.A. Zaykoski, S.J. Causey  
**Mechanical, thermal, and oxidation properties of refractory hafnium and zirconium compounds**  
J. Eur. Ceram. Soc., 19 (1999), pp. 2405-2414, [10.1016/S0955-2219\(99\)00129-6](#)  
[Article](#)  [Download PDF](#)   [View Record in Scopus](#)   [Google Scholar](#)
- [2] S.R. Levine, E.J. Opila, M.C. Halbig, J.D. Kiser, M. Singh, J.A. Salem  
**Evaluation of ultra-high temperature ceramics for aeropropulsion use**  
J. Eur. Ceram. Soc., 22 (2002), pp. 2757-2767, [10.1016/S0955-2219\(02\)00140-1](#)  
[Article](#)  [Download PDF](#)   [View Record in Scopus](#)   [Google Scholar](#)
- [3] J.J. Sha, J. Li, S.H. Wang, Z.F. Zhang, Y.F. Zu, S. Flauder, *et al.*


**Improved microstructure and fracture properties of short carbon fiber-toughened ZrB<sub>2</sub>-based UHTC composites via colloidal process**

Int. J. Refract. Met. Hard Mater., 60 (2016), pp. 68-74, [10.1016/j.ijrmhm.2016.07.010](https://doi.org/10.1016/j.ijrmhm.2016.07.010)

[Article](#)  [Download PDF](#) [View Record in Scopus](#) [Google Scholar](#)


- [4] W.G. Fahrenholtz, G.E. Hilmas, I.G. Talmy, J.A. Zaykoski  
**Refractory diborides of zirconium and hafnium**  
J. Am. Ceram. Soc., 90 (2007), pp. 1347-1364, [10.1111/j.1551-2916.2007.01583.x](https://doi.org/10.1111/j.1551-2916.2007.01583.x)  
[CrossRef](#) [View Record in Scopus](#) [Google Scholar](#)
- [5] T.A. Parthasarathy, R.A. Rapp, M. Opeka, R.J. Kerans  
**A model for the oxidation of ZrB<sub>2</sub>, HfB<sub>2</sub> and TiB<sub>2</sub>**  
Acta Mater., 55 (2007), pp. 5999-6010, [10.1016/j.actamat.2007.07.027](https://doi.org/10.1016/j.actamat.2007.07.027)  
[Article](#)  [Download PDF](#) [View Record in Scopus](#) [Google Scholar](#)
- [6] L. Silvestroni, G. Meriggi, D. Sciti  
**Oxidation behavior of ZrB<sub>2</sub> composites doped with various transition metal silicides**  
Corros. Sci., 83 (2014), pp. 281-291, [10.1016/j.corsci.2014.02.026](https://doi.org/10.1016/j.corsci.2014.02.026)  
[Article](#)  [Download PDF](#) [View Record in Scopus](#) [Google Scholar](#)
- [7] L. Zoli, D. Sciti  
**Efficacy of a ZrB<sub>2</sub>/SiC matrix in protecting C fibres from oxidation in novel UHTCMC materials**  
Mater. Des., 113 (2017), pp. 207-213, [10.1016/j.matdes.2016.09.104](https://doi.org/10.1016/j.matdes.2016.09.104)  
[Article](#)  [Download PDF](#) [View Record in Scopus](#) [Google Scholar](#)
- [8] A. Vinci, L. Zoli, E. Landi, D. Sciti  
**Oxidation behaviour of a continuous carbon fibre reinforced ZrB<sub>2</sub>-SiC composite**  
Corros. Sci. (2017), [10.1016/j.corsci.2017.04.012](https://doi.org/10.1016/j.corsci.2017.04.012)  
[Google Scholar](#)
- [9] A. Balbo, D. Sciti  
**Spark plasma sintering and hot pressing of ZrB<sub>2</sub>-MoSi<sub>2</sub> ultra-high-temperature ceramics**  
Mater. Sci. Eng. A, 475 (2008), pp. 108-112, [10.1016/j.msea.2007.01.164](https://doi.org/10.1016/j.msea.2007.01.164)  
[Article](#)  [Download PDF](#) [View Record in Scopus](#) [Google Scholar](#)
- [10] M. Mashhadi, H. Khaksari, S. Safi  
**Pressureless sintering behavior and mechanical properties of ZrB<sub>2</sub> - SiC composites: effect of SiC content and particle size**  
Integr Med Res, 4 (2015), pp. 416-422, [10.1016/j.jmrt.2015.02.004](https://doi.org/10.1016/j.jmrt.2015.02.004)  
[Article](#)  [Download PDF](#) [View Record in Scopus](#) [Google Scholar](#)
- [11] S. Tang, J. Deng, S. Wang, W. Liu, K. Yang  
**Ablation behaviors of ultra-high temperature ceramic composites**  
Mater. Sci. Eng. A, 465 (2007), pp. 1-7, [10.1016/j.msea.2007.02.040](https://doi.org/10.1016/j.msea.2007.02.040)

- [12] S. Tang, J. Deng, S. Wang, W. Liu  
**Comparison of thermal and ablation behaviors of C/SiC composites and C/ZrB<sub>2</sub>-SiC composites**  
Corros. Sci., 51 (2009), pp. 54-61, [10.1016/j.corsci.2008.09.037](https://doi.org/10.1016/j.corsci.2008.09.037)  
[Article](#)  [Download PDF](#) [View Record in Scopus](#) [Google Scholar](#)
- [13] D. Sciti, A. Natali Murri, V. Medri, L. Zoli  
**Continuous C fibre composites with a porous ZrB<sub>2</sub> matrix**  
Mater. Des., 85 (2015), pp. 127-134, [10.1016/j.matdes.2015.06.136](https://doi.org/10.1016/j.matdes.2015.06.136)  
[Article](#)  [Download PDF](#) [View Record in Scopus](#) [Google Scholar](#)
- [14] D. Sciti, L. Pienti, A. Natali Murri, E. Landi, V. Medri, L. Zoli  
**From random chopped to oriented continuous SiC fibers-ZrB<sub>2</sub> composites**  
Mater. Des., 63 (2014), pp. 464-470, [10.1016/j.matdes.2014.06.037](https://doi.org/10.1016/j.matdes.2014.06.037)  
[Article](#)  [Download PDF](#) [View Record in Scopus](#) [Google Scholar](#)
- [15] L. Zoli, D. Sciti  
**Efficacy of a ZrB<sub>2</sub>-SiC matrix in protecting C fibres from oxidation in novel UHTCMC materials**  
Mater. Des., 113 (2017), pp. 207-213, [10.1016/j.matdes.2016.09.104](https://doi.org/10.1016/j.matdes.2016.09.104)  
[Article](#)  [Download PDF](#) [View Record in Scopus](#) [Google Scholar](#)
- [16] A. Vinci, L. Zoli, E. Landi, D. Sciti  
**Oxidation behaviour of a continuous carbon fibre reinforced ZrB<sub>2</sub>-SiC composite**  
Corros. Sci., 123 (2017), [10.1016/j.corsci.2017.04.012](https://doi.org/10.1016/j.corsci.2017.04.012)  
[Google Scholar](#)
- [17] L. Silvestroni, D. Dalle Fabbriche, C. Melandri, D. Sciti  
**Relationships between carbon fiber type and interfacial domain in ZrB<sub>2</sub>-based ceramics**  
J. Eur. Ceram. Soc., 36 (2016), pp. 17-24, [10.1016/j.jeurceramsoc.2015.09.026](https://doi.org/10.1016/j.jeurceramsoc.2015.09.026)  
[Article](#)  [Download PDF](#) [View Record in Scopus](#) [Google Scholar](#)
- [18] Berk  
**Classification and regression trees**  
Data Min with R Art Excav Data Knowl Discov Use R (2009), pp. 36-350, [10.1007/s00038-011-0315-z](https://doi.org/10.1007/s00038-011-0315-z)  
[View Record in Scopus](#) [Google Scholar](#)
- [19] A.M. Prasad, L.R. Iverson, A. Liaw  
**Newer classification and regression tree techniques: bagging and random forests for ecological prediction**  
Ecosystems, 9 (2006), pp. 181-199, [10.1007/s10021-005-0054-1](https://doi.org/10.1007/s10021-005-0054-1)  
[CrossRef](#) [View Record in Scopus](#) [Google Scholar](#)

- [20] G. De'ath, K.E. Fabricius  
**Classification and regression trees: a powerful yet simple technique for ecological data analysis**  
Ecology, 81 (2000), pp. 3178-3192, [10.1890/0012-9658\(2000\)081\[3178:CARTAP\]2.0.CO;2](https://doi.org/10.1890/0012-9658(2000)081[3178:CARTAP]2.0.CO;2)  
[CrossRef](#) [View Record in Scopus](#) [Google Scholar](#)
- [21] J.R. Leathwick, J. Elith, M.P. Francis, T. Hastie, P. Taylor  
**Variation in demersal fish species richness in the oceans surrounding New Zealand: an analysis using boosted regression trees**  
Mar. Ecol. Prog. Ser., 321 (2006), pp. 267-281, [10.3354/meps321267](https://doi.org/10.3354/meps321267)  
[CrossRef](#) [View Record in Scopus](#) [Google Scholar](#)
- [22] P. Tittoneil, K. Shepherd, B. Vanlauwe, K. Giller  
**Unravelling the effects of soil and crop management on maize productivity in smallholder agricultural systems of western Kenya—an application of classification and regression tree analysis**  
Agric. Ecosyst. Environ., 123 (2008), pp. 137-150, [10.1016/j.agee.2007.05.005](https://doi.org/10.1016/j.agee.2007.05.005)  
[Article](#)  [Download PDF](#) [View Record in Scopus](#) [Google Scholar](#)
- [23] G.C. Fonarow, K.F. Adams, W.T. Abraham, W. Clyde, W.J.B. Yancy  
**Risk stratification for in-hospital mortality in acutely decompensated heart failure classification and regression tree analysis**  
J. Am. Med. Assoc., 293 (2005), pp. 572-580  
[CrossRef](#) [View Record in Scopus](#) [Google Scholar](#)
- [24] S.C. Lemon, J. Roy, M.A. Clark, P.D. Friedmann, W. Rakowski  
**Classification and regression tree analysis in public health: methodological review and comparison with logistic regression**  
Ann. Behav. Med., 26 (2003), pp. 172-181, [10.1207/S15324796ABM2603\\_02](https://doi.org/10.1207/S15324796ABM2603_02)  
[CrossRef](#) [View Record in Scopus](#) [Google Scholar](#)
- [25] J.H. Friedman, J.J. Meulman  
**Multiple additive regression trees with application in epidemiology**  
Stat. Med., 22 (2003), pp. 1365-1381, [10.1002/sim.1501](https://doi.org/10.1002/sim.1501)  
[CrossRef](#) [View Record in Scopus](#) [Google Scholar](#)
- [26] P.C. Austin  
**A comparison of regression trees, logistic regression, generalized additive models, and multivariate adaptive regression splines for predicting AMI mortality**  
Stat. Med., 26 (2007), pp. 2937-2957, [10.1002/sim.2770](https://doi.org/10.1002/sim.2770)  
[CrossRef](#) [View Record in Scopus](#) [Google Scholar](#)
- [27] C. Strobl, J. Malley, G. Tutz  
**An introduction to recursive partitioning: rationale, application, and characteristics of classification and regression trees, bagging, and random forests**  
Psychol. Methods (2009), [10.1037/a0016973](https://doi.org/10.1037/a0016973)  
[Google Scholar](#)
- [28] E. Gervilla, A. Palmer  
**Prediction of cannabis and cocaine use in adolescence using decision trees and logistic regression**

Eur J Psychol Appl to Leg Context, 2 (1) (2010), pp. 19-35

[View Record in Scopus](#) [Google Scholar](#)

- [29] S.B. Scott, B.R. Whitehead, C.S. Bergeman, L. Pitzer  
**Combinations of stressors in midlife: examining role and domain stressors using regression trees and random forests**  
J. Gerontol. B Psychol. Sci. Soc. Sci., 68 (2013), pp. 464-475, [10.1093/geronb/gbs166](#)  
[CrossRef](#) [View Record in Scopus](#) [Google Scholar](#)
- [30] G. Giorgi, D. Dubin, J.F. Perez  
**Perceived organizational support for enhancing welfare at work: a regression tree model**  
Front. Psychol., 7 (2016), Article 1770, [10.3389/fpsyg.2016.01770](#)  
[Google Scholar](#)
- [31] Y. Li  
**Predicting materials properties and behavior using classification and regression trees**  
Mater. Sci. Eng. A, 433 (2006), pp. 261-268, [10.1016/j.msea.2006.06.100](#)  
Article  [Download PDF](#) [View Record in Scopus](#) [Google Scholar](#)
- [32] I. Mansouri, T. Ozbakkaloglu, O. Kisi, T. Xie  
**Predicting behavior of FRP-confined concrete using neuro fuzzy, neural network, multivariate adaptive regression splines and M5 model tree techniques**  
Mater. Struct., 49 (2016), pp. 4319-4334, [10.1617/s11527-015-0790-4](#)  
[CrossRef](#) [View Record in Scopus](#) [Google Scholar](#)
- [33] D.G. Munz, J.L. Shannon, R.T. Bubsey  
**Fracture toughness calculation from maximum load in four point bend tests of chevron notch specimens**  
Int. J. Fract., 16 (1980), [10.1007/BF00013393](#)  
[Google Scholar](#)
- [34] B. Lantz  
**Machine Learning with R**  
(Second Edition) (2015)  
[Google Scholar](#)
- [35] L. Breiman  
**Random forests**  
Mach. Learn., 45 (2001), pp. 5-32, [10.1023/A:1010933404324](#)  
[CrossRef](#) [View Record in Scopus](#) [Google Scholar](#)
- [36] C. Yu-Wei, C. David  
**Machine Learning with R Cookbook**  
(2015)  
[Google Scholar](#)

- [37] S.S. Hwang, A.L. Vasiliev, N.P. Padture  
**Improved processing and oxidation-resistance of ZrB<sub>2</sub> ultra-high temperature ceramics containing SiC nanodispersoids**  
Mater. Sci. Eng. A, 464 (2007), pp. 216-224, [10.1016/j.msea.2007.03.002](https://doi.org/10.1016/j.msea.2007.03.002)  
[Article](#) [Download PDF](#) [CrossRef](#) [View Record in Scopus](#) [Google Scholar](#)
- [38] S.C. Zhang, G.E. Hilmas, W.G. Fahrenholtz  
**Mechanical properties of sintered ZrB<sub>2</sub>-SiC ceramics**  
J. Eur. Ceram. Soc., 31 (2011), pp. 893-901, [10.1016/j.jeurceramsoc.2010.11.013](https://doi.org/10.1016/j.jeurceramsoc.2010.11.013)  
[Article](#) [Download PDF](#) [View Record in Scopus](#) [Google Scholar](#)
- [39] J. Watts, G. Hilmas, W.G. Fahrenholtz  
**Mechanical characterization of ZrB<sub>2</sub>-SiC composites with varying SiC particle sizes**  
J. Am. Ceram. Soc., 94 (2011), pp. 4410-4418, [10.1111/j.1551-2916.2011.04885.x](https://doi.org/10.1111/j.1551-2916.2011.04885.x)  
[CrossRef](#) [View Record in Scopus](#) [Google Scholar](#)
- [40] F. Monteverde, S. Guicciardi, A. Bellosi  
**Advances in microstructure and mechanical properties of zirconium diboride based ceramics**  
Mater. Sci. Eng. A, 346 (2003), pp. 310-319, [10.1016/S0921-5093\(02\)00520-8](https://doi.org/10.1016/S0921-5093(02)00520-8)  
[Article](#) [Download PDF](#) [View Record in Scopus](#) [Google Scholar](#)
- [41] E.W. Neuman, G.E. Hilmas, W.G. Fahrenholtz  
**Mechanical behavior of zirconium diboride-silicon carbide ceramics at elevated temperature in air**  
J. Eur. Ceram. Soc., 33 (2013), pp. 2889-2899, [10.1016/j.jeurceramsoc.2013.05.003](https://doi.org/10.1016/j.jeurceramsoc.2013.05.003)  
[Article](#) [Download PDF](#) [View Record in Scopus](#) [Google Scholar](#)
- [42] A.L. Chamberlain, W.G. Fahrenholtz, G.E. Hilmas, D.T. Ellerby  
**High-strength zirconium diboride-based ceramics**  
J. Am. Ceram. Soc., 87 (2004), pp. 1170-1172  
(Cited By (since 1996) 255\nExport Date 14 June 2012)  
[CrossRef](#) [View Record in Scopus](#) [Google Scholar](#)
- [43] Y.-J. Lee  
**Formation of silicon carbide on carbon fibers by carbothermal reduction of silica**  
Diam. Relat. Mater., 13 (2004), pp. 383-388, [10.1016/j.diamond.2003.11.062](https://doi.org/10.1016/j.diamond.2003.11.062)  
[Article](#) [Download PDF](#) [View Record in Scopus](#) [Google Scholar](#)
- [44] A.G. Evans, F.W. Zok  
**The physics and mechanics of fibre-reinforced brittle matrix composites**  
J. Mater. Sci., 29 (1994), pp. 3857-3896, [10.1007/BF00355946](https://doi.org/10.1007/BF00355946)  
[CrossRef](#) [View Record in Scopus](#) [Google Scholar](#)
- [45] C. Yue, W. Liu, L. Zhang, T. Zhang, Y. Chen

**Fracture toughness and toughening mechanisms in a (ZrB<sub>2</sub>-SiC) composite reinforced with boron nitride nanotubes and boron nitride nanoplatelets**

Scr. Mater., 68 (2013), pp. 579-582, [10.1016/j.scriptamat.2012.12.005](https://doi.org/10.1016/j.scriptamat.2012.12.005)

[Article](#)  [Download PDF](#) [View Record in Scopus](#) [Google Scholar](#)

[46] M.S. Asl, M.G. Kakroudi, S. Noori

**Hardness and toughness of hot pressed ZrB<sub>2</sub>-SiC composites consolidated under relatively low pressure**

J. Alloys Compd., 619 (2015), pp. 481-487, [10.1016/j.jallcom.2014.09.006](https://doi.org/10.1016/j.jallcom.2014.09.006)

[Article](#)  [Download PDF](#) [Google Scholar](#)

[47] K. Gui, P. Hu, W. Hong, X. Zhang, S. Dong

**Microstructure, mechanical properties and thermal shock resistance of ZrB<sub>2</sub>-SiC-C f composite with inhibited degradation of carbon fibers**

J. Alloys Compd., 706 (2017), pp. 16-23, [10.1016/j.jallcom.2017.02.227](https://doi.org/10.1016/j.jallcom.2017.02.227)

[Article](#)  [Download PDF](#) [View Record in Scopus](#) [Google Scholar](#)

[48] W.M. Guo, Y. You, G.J. Zhang, S.H. Wu, H.T. Lin

**Improvement of fracture toughness of ZrB<sub>2</sub>-SiC composites with carbon interfaces**

J. Eur. Ceram. Soc., 35 (2015), pp. 1985-1989, [10.1016/j.jeurceramsoc.2014.12.026](https://doi.org/10.1016/j.jeurceramsoc.2014.12.026)

[Article](#)  [Download PDF](#) [View Record in Scopus](#) [Google Scholar](#)

[49] L. Zoli, A. Vinci, L. Silvestroni, D. Sciti, M. Reece, S. Grasso

**Rapid spark plasma sintering to produce dense UHTCs reinforced with undamaged carbon fibres**

Mater. Des., 130 (2017), [10.1016/j.matdes.2017.05.029](https://doi.org/10.1016/j.matdes.2017.05.029)

[Google Scholar](#)

[50] W. Hong, K. Gui, P. Hu, X. Zhang, S. Dong

**Preparation and characterization of high-performance ZrB<sub>2</sub>-SiC-Cf composites sintered at 1450 °C**

J. Adv. Ceram., 6 (2017), pp. 110-119, [10.1007/s40145-017-0223-7](https://doi.org/10.1007/s40145-017-0223-7)

[CrossRef](#) [View Record in Scopus](#) [Google Scholar](#)

[51] J. Lamon

**Interfaces and interfacial mechanics: influence on the mechanical behavior of ceramic matrix composites (CMC)**

J. Phys. (1993), pp. 3:1607-16, [10.1051/jp4:19937252](https://doi.org/10.1051/jp4:19937252)

[Google Scholar](#)

[52] A.G. Evans, D.B. Marshall

**Overview no. 85: The mechanical behavior of ceramic matrix composites**

Acta Metall., 37 (1989), pp. 2567-2583, [10.1016/0001-6160\(89\)90291-5](https://doi.org/10.1016/0001-6160(89)90291-5)

[Article](#)  [Download PDF](#) [View Record in Scopus](#) [Google Scholar](#)

[53] T.L. Jessen, B.A. Bender, V.A. Greenhut

**Effect of bridged boron nitride coatings on the flexure behavior of a unidirectional ceramic-fiber ceramic-matrix composite**

J. Am. Ceram. Soc., 83 (2000), pp. 3231-3233, [10.1111/j.1151-2916.2000.tb01715.x](https://doi.org/10.1111/j.1151-2916.2000.tb01715.x)



